Supplementary Figure Legends

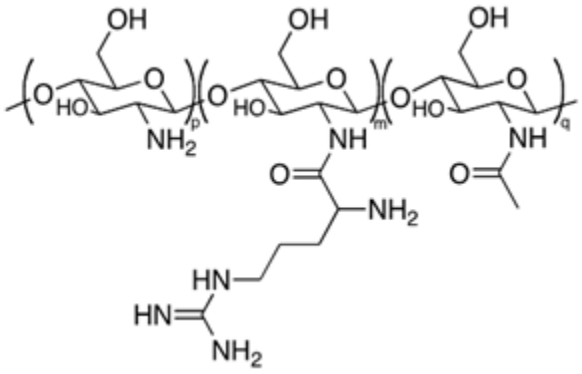

Supplementary Figure 1. Structure of PAAG molecule.

Supplemental 2

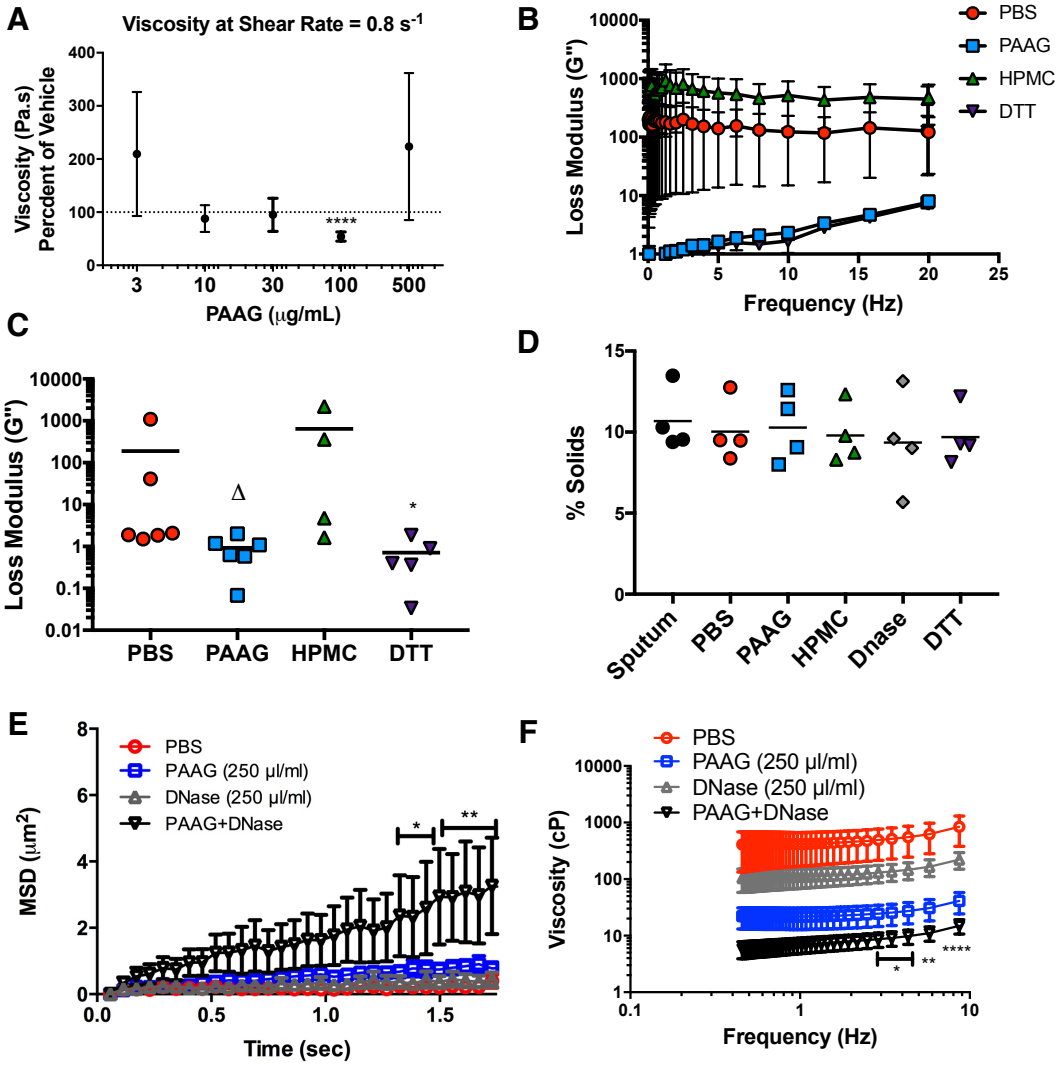

Supplementary Figure 2. Effect of PAAG on mucus viscosity on primary CF HBE cells *in situ*. A: Dose response data over 2-logs at half log increments. **B:** Loss modulus (G") over a frequency sweep of expectorated CF sputum samples incubated with PBS, PAAG (100 μg/ml), HPMC control, or DTT control. **C:** Summary data of loss modulus derived from A, at a frequency of 0.8 Hz. $^{\Delta}p=0.07$ **D:** Percent (%) solids measurements of sputum samples with enough volume were taken in conjunction with viscoelastic measurements in Figure 1E (n=4

donors). **E-F:** Phe508del/Phe508del HBE cells treated with PAAG, the mucolytic, DNAse or PAAG/DNase combination (10 µl of 5 mg/ml PAAG or DNAse added apically, to achieve 250 µg/ml final concentration, respectively, in the ASL), as compared to PBS control. Additions performed 24 hours prior to assay. Summary data demonstrating particle mean square displacement (E) and effective viscosity over a range of frequencies (F). *P<0.05, **P<0.01, ****P<0.0001 by one-way or two-way ANOVA.

Supplemental 3

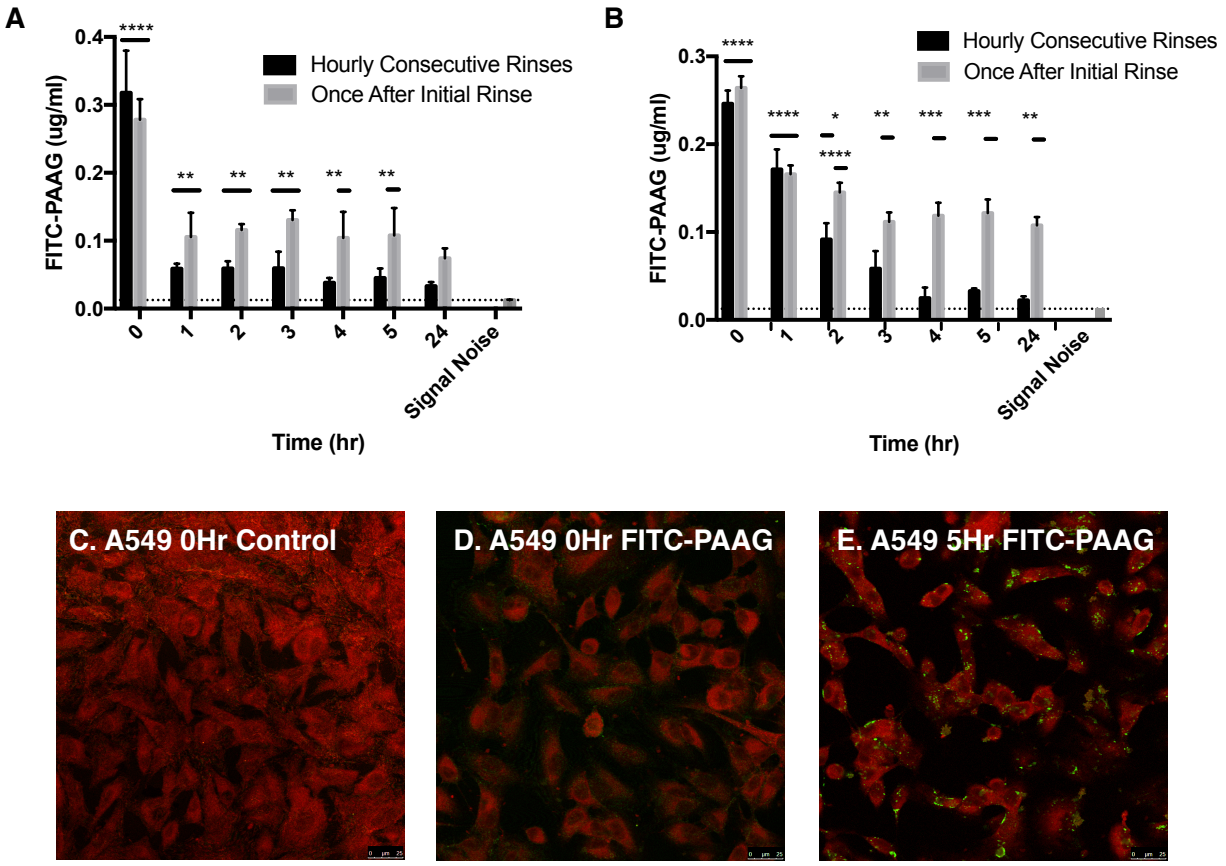

Supplemental Figure 3. PAAG adheres to human lung epithelial cells. A: PAAG-FITC (at 200 µg/mL) was applied to A549 human lung epithelial cells for 30 minutes, then the cells were serially rinsed at each time point (hourly) or once, at the initial time point only. Detection of FITC-PAAG on the surface of the cells is plotted, as compared to no PAAG control (dotted line). **B:** Same experiment as in *A,* conducted with differentiated A431 skin epithelial cells. Summary data derived from 12 replicates. **C-E:** Representative images from *A*, Control at 0 hours (C), FITC-PAAG at 0 hours (D), and FITC-PAAG at 5 hours after a single wash (E). *P ≤ 0.05, **P≤ 0.01, ****P≤ 0.0001 vs. no PAAG control.

Supplemental 4

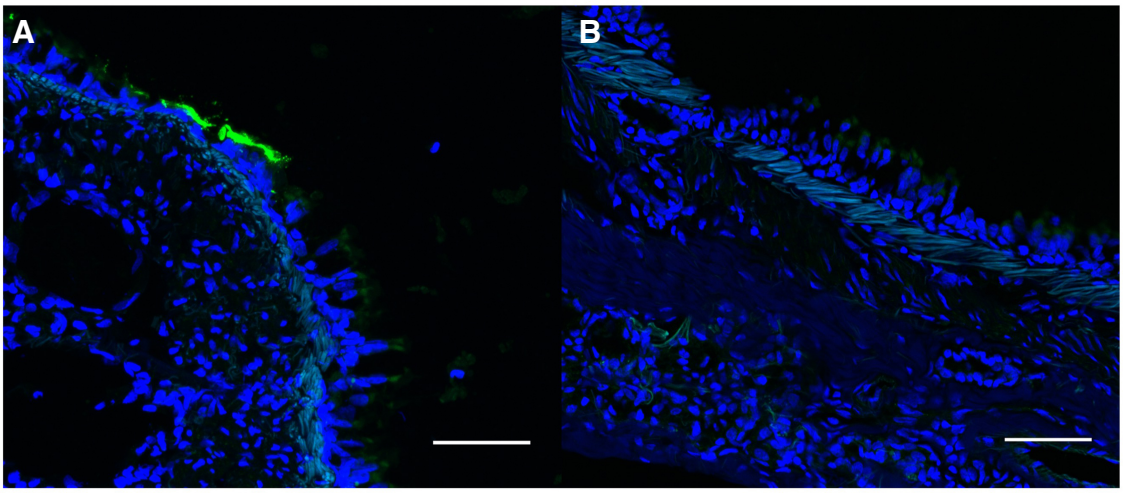

Supplementary Figure 4*. In vivo* localization of PAAG. A-B. Aerosolized FITC-PAAG (A) or PAAG (B) was nebulized to wild-type ferrets and lungs were examined under confocal microscopy. FITC-PAAG deposits heterogeneously in clumps on airway epithelia *in vivo.* Scale bar = 50 μm.

Supplemental 5

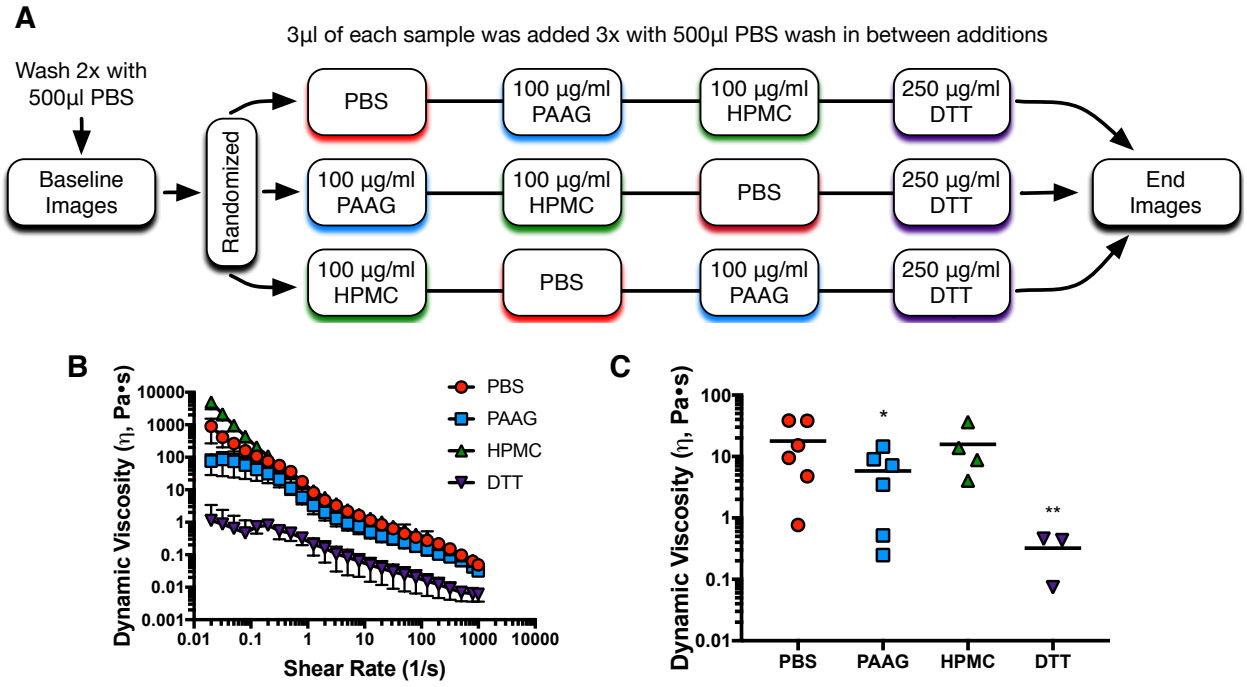

Supplementary Figure 5. PAAG reduces viscosity of CF sputum. A: Expectorated CF sputum was treated with PAAG, HPMC, DTT (each 100 µg/ml x 2 hrs), or PBS control, and then added to the surface of freshly excised rat trachea while monitoring by µOCT. Order of sample addition was randomized in each experiment. **B-C:** Dynamic viscosity (η) curves (B) and summary data at a frequency of 0.8 Hz (C) of CF sputum with the treatments reported in *A*. *P ≤ 0.05, **P≤ 0.01 by Kruskal Wallis test with Dunn's MCT.

Supplemental 6

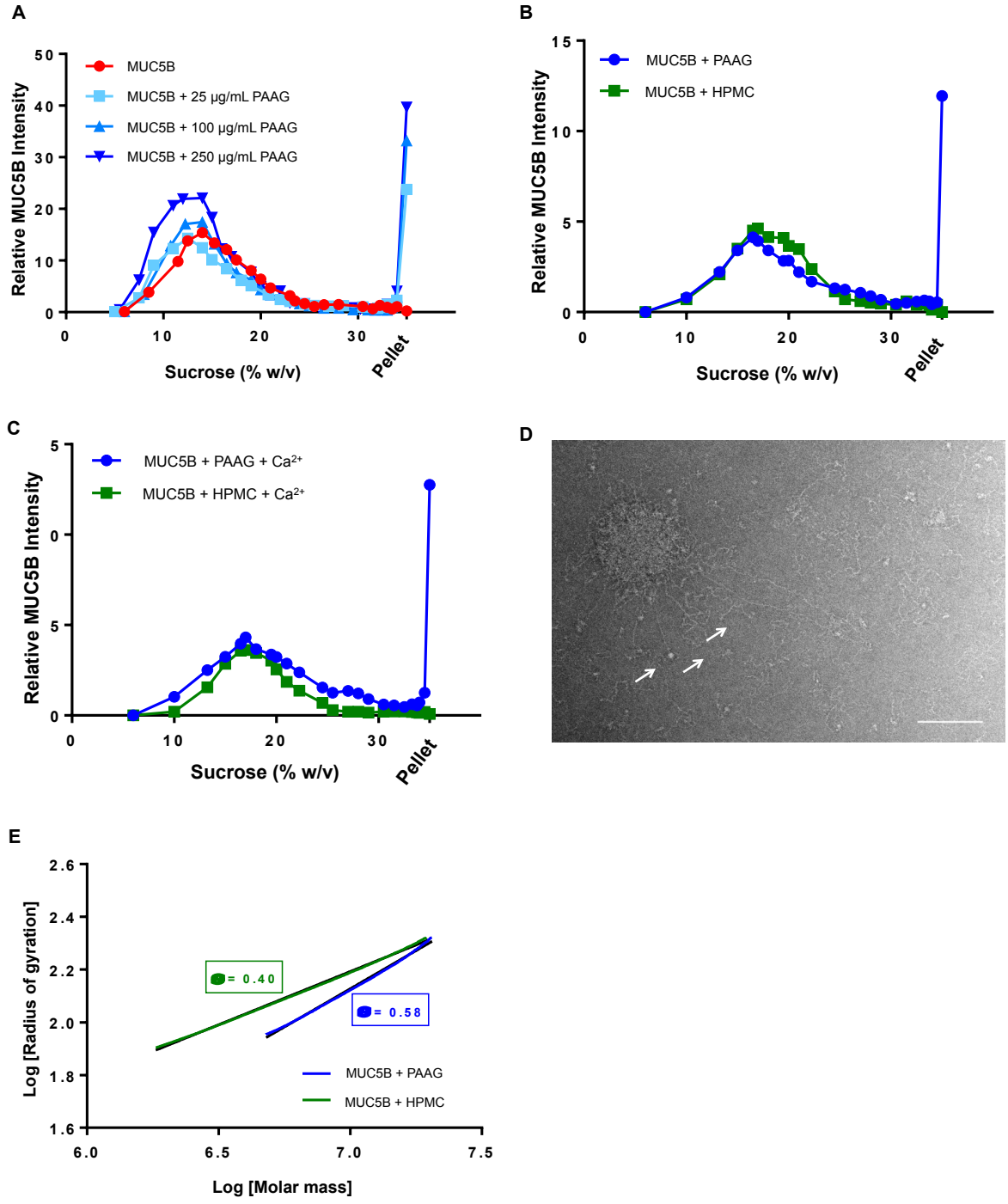

Supplementary Figure 6. PAAG alters conformation of MUC5B. The effects of PAAG on the sedimentation behavior of 150 µg/ml MUC5B was assessed using rate zonal centrifugation and TEM, scale bars = 200 nm. **A:** MUC5B incubated with a range of PAAG concentrations (0, 25,

100, 250 µg/ml) resulted in a changing mucin sedimentation profile. **B-C:** MUC5B incubated with either 100 µg/ml PAAG or 100 µg/ml HMPC showed that PAAG but not HPMC affected the sedimentation behavior of MUC5B (B). Faster sedimenting MUC5B was also observed in the presence and absence of Ca^{2+}, although PAAG also induced increased formation of slower sedimenting MUC5B (C). **D:** Visualization of faster sedimenting MUC5B imaged using TEM. These polymers displayed highly linearized MUC5B molecules organized around aggregates as highlighted by white arrows, whereas slower sedimenting MUC5B showed a normal network appearance visualized by TEM (Fig 3B). **E:** The molecular shape of MUC5B (assessed by value of α, the Marck-Houwinck shape parameter[59] which can be used as an index of molecular stiffness. **E:** The molecular shape of MUC5B (assessed by value of α, the Marck-Houwinck shape parameter[65] which can be used as an index of molecular stiffness. α values closer to 1 represent more rod-like molecules, 0.5–0.6 for random coils and 0.33 for compact spheres) after treatment with PAAG (100 µg/ml) exhibited a more extended conformation in solution (compared to HMPC-treated MUC5B) which in agreement with the more linear mucins visualized by TEM (Fig 3B), n = 3/condition.

Supplemental 7

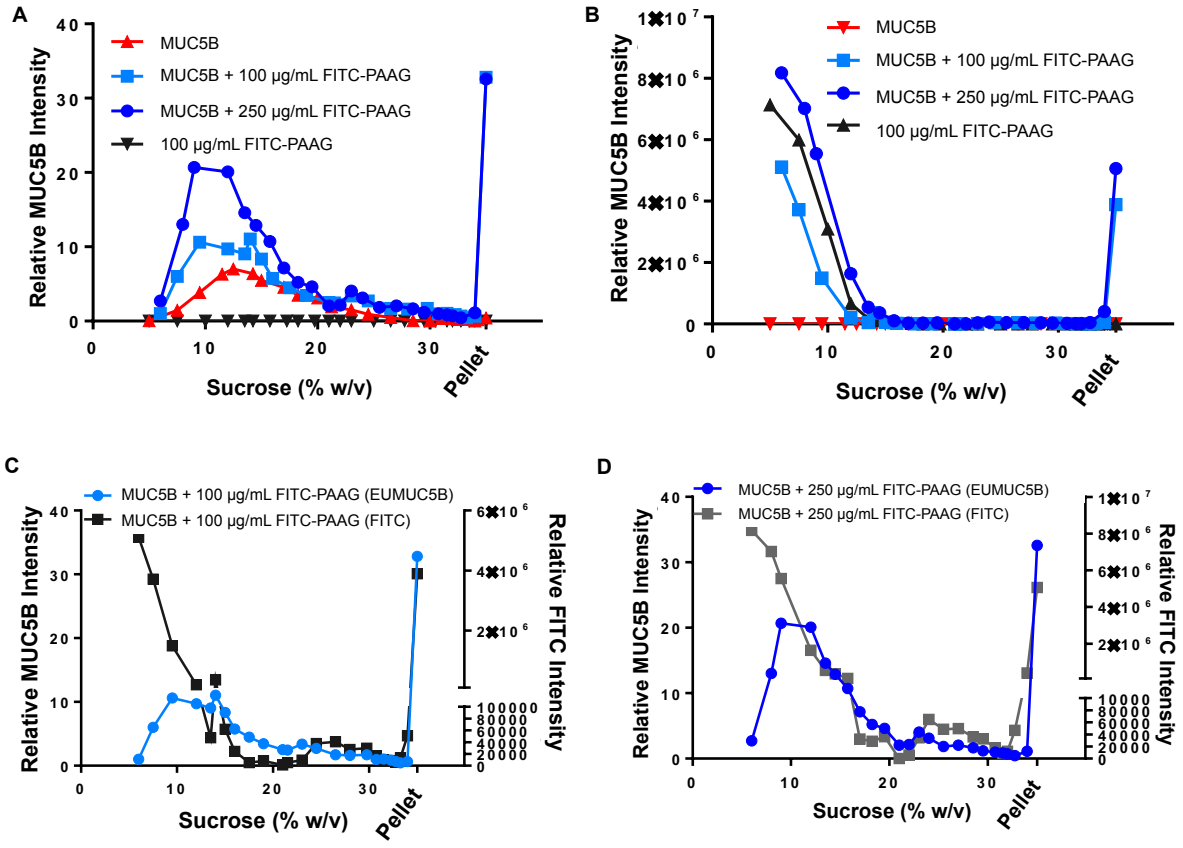

Supplemental Figure 7. FITC-PAAG co-sediments with MUC5B. To assess the interaction of PAAG with MUC5B we performed rate-zonal centrifugation experiments using 150 µgµg/ml MUC5B in the presence of FITC-labeled PAAG at varying concentrations (0, 100, 250 µgµg/ml). **A:** MUC5B incubated with FITC-PAAG exhibited a change in its sedimentation profile, similar to that observed with unlabeled PAAG. In the presence of FITC-PAAG the majority of MUC5B polymers were seen to sediment at ~8 % sucrose compared to ~13% for untreated molecules. In addition only in the presence either PAAG (S5A-C) or FITC-PAAG were MUC5B polymers seen to pellet. **B:** FITC-PAAG changes its sedimentation behavior only in the presence of MUC5B as highlighted through a dramatic increase in pelleted material. **C-D:** By overlaying the sedimentation profiles of MUC5B and FITC-PAAG we observed co-sedimentation between the two molecules as highlighted by the similarity in the traces, demonstrating a potential interaction

between the two molecules. Y-axes scales were expanded to highlight the co-sedimentation of FITC-PAAG with MUC5B, n = 3/condition.

Supplemental 8

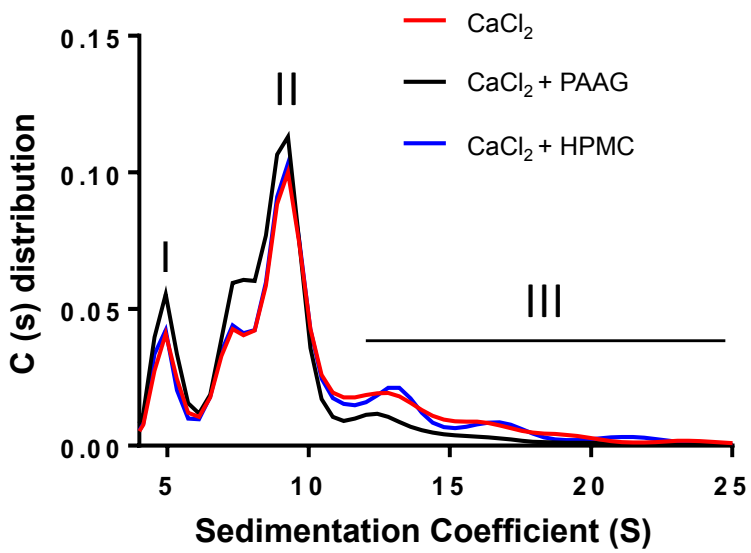

Supplemental Figure 8. pH-dependent, calcium-mediated N-terminal MUC5B multimerization was reversed upon addition of PAAG. Recombinant dimer-enriched N-terminal MUC5B (NT5B) was incubated with 10 mM $CaCl_2$ at pH 5.5 (red) to form multimers. This sample was split and PAAG (100 µg/ml, black) or HMPC (100 µg/ml, blue) was added. Representative profiles following AUC analysis showed peaks corresponding to monomer (I), dimer (II) and larger multimers (III). The calcium-mediated multimerization of NT5B, was maintained following incubation with HMPC, but reversed upon addition of PAAG, n=3/condition. The loss of NT5B multimers caused by PAAG was similar to that reported for the disruption of the non-covalent, calcium-dependent assemblies of NT5B dimers caused by the calcium sequestering reagent, EGTA.[29]

Supplemental 9

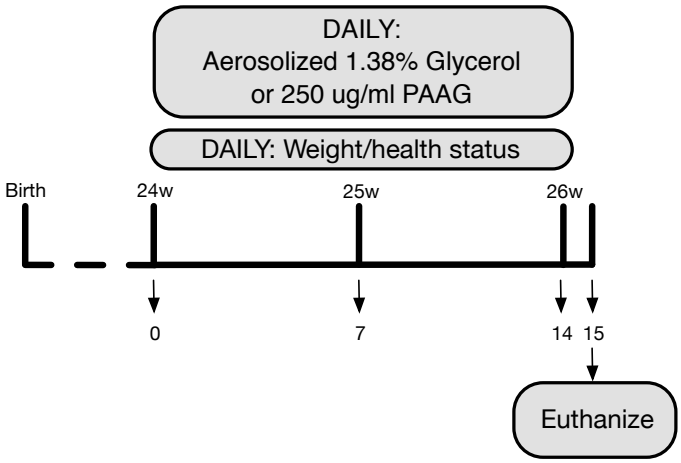

Supplemental Figure 9. In vivo nebulization of PAAG to 6-month-old Cftr$^{-/-}$ rats. Schematic of experimental protocol for 14-day treatment of PAAG.

Video 1. Transport of PBS-treated CF sputum. PBS-treated CF sputum (3 µl) was added to a non-CF rat trachea. Sputum transport rate was visualized using µOCT based imaging.

Video 2. Transport of PAAG-treated CF sputum. PAAG-treated (100 µg/ml) CF sputum (3 µl) was added to a non-CF rat trachea. Sputum transport rate was visualized using µOCT based imaging.

Video 3. MCT of Vehicle-treated $Cftr^{-/-}$ rats. Mucus transport in Vehicle-treated $Cftr^{-/-}$ rats was visualized using µOCT based imaging.

Video 4. Transport of PAAG-treated $Cftr^{-/-}$ rats. Mucus transport in PAAG-treated $Cftr^{-/-}$ rats was visualized using µOCT based imaging.

Supplementary Tables

Supplementary Table 1: Subject demographics. Data are presented as n (percentage of total) or median (range).

Table 1: Subject Demographics (n=11)	
Age	33.9 (21-53)
Gender (Female)	4 (36.4%)
BMI	20.2 (19-28.6)
Genotype	
F508del homozygous	4 (36.4%)
F508del heterozygous	6 (54.5%)
Other	1 (9.1%)
FEV1 (%)	58% (15-87%)
PULMOZYME®	10 (90.9%)
Pseudomonas aeruginosa Mucoid	10 (90.9%)

S. Table 2. Proteomic analysis of ferret bronchoalveolar lavage fluid. Selected proteins – see online repository for complete dataset. Fold change indicates change after PAAG treatment with respect to pretreatment baseline, data from n-3 ferrets.

Identified Proteins	Gene Symbol	Fold Change	T-test (p-value)
mucin-5B [Mustela putorius furo]	MUC5B	- 2.9	< 0.0001
myeloperoxidase [Mustela putorius furo]	MPO	- 4.2	< 0.0001
neutrophil elastase [Mustela putorius furo]	ELANE	- 8.5	0.0056
neutrophil collagenase isoform X1 [Mustela putorius furo]	MMP8	- 4.5	< 0.0001
protein S100-A8 [Mustela putorius furo]	S100A8	- 3.3	< 0.0001
protein S100-A9 [Mustela putorius furo]	S100A9	- 4.3	< 0.0001